

## Stress Analysis in Structural Components of the Koepe Pulley in Hoisting Installations

Stanisław WOLNY, Sławomir BADURA

*AGH University of Science and Technology  
Faculty of Mechanical Engineering and Robotics  
Al. Mickiewicza 30, 30-059, Kraków, Poland  
e-mail: {stwolny, sbadura}@agh.edu.pl*

Hoisting installations in mines have been constructed and operated for many years, yet they still merit a rigorous research to identify all factors that would enable us to improve their performance parameters. A Koepe pulley in a winding system is a complex structural component, made of plates, shells, discs, membranes, radial or circumferential fin elements varying in their actual layout, depending on the design.

The strength analysis of a Koepe pulley in a hoisting system is carried out to get a better insight into the state of stress experienced by pulley components under the operational loads and to find the extreme values of the stress components, which underlies the fatigue endurance and life assessments.

Accordingly, the stress analysis of pulley elements is performed by the numerical methods, utilising the FEM approach. Models are developed using the program “FEMAP” and the stress analysis uses the package “NE” / “Nastran for Windows”.

The numerical data are then verified through strain (stress) measurements taken on a real object, under the typical operating conditions.

**Key words:** mine hoist, Koepe pulley, dynamics, stress.

### 1. INTRODUCTION

Koepe pulley and other assemblies of the hoisting installations (conveyances, suspensions of conveyances and hoisting ropes) are spatial structures incorporating various elements in the shape of beams, discs, panels or shell structures exhibiting an intricate outer edge configuration, and having apertures, mostly circular in shape, to fix ropes and the components of the guiding system [1, 2]. Finding the stress distribution and stress concentration factors in those elements becomes a complicated problem involving the theory of elasticity whilst under the mining laws currently in force these components are to be dimensioned by

the admissible stress method, taking into account the maximal static loads experienced when in service.

Stress values calculated in characteristic cross-sections of these constructions and based on fundamental formulas and calculation schemes (rods under tension, free-ends beams) are compared with admissible stress levels defined in line with safety factors as required by the relevant mining laws [1].

However, our knowledge of the actual state of stress generated in Koepe pulley components is far from complete and hence forecasting their service life seems problematic, if not wholly impossible.

That is why the endurance analysis is performed of Koepe pulley components using the numerical methods and taking into account the real service loads.

The results are verified by comparing the numerical data to measurements taken on a real object. Stress and strain is measured at the points that experienced the maximal effort, as revealed by the numerical results.

## 2. ENDURANCE ANALYSIS OF A KOEPE PULLEY IN A HOISTING SYSTEM

Endurance analysis is performed of a Koepe pulley in a hoisting installation shown schematically in Fig 1. The key operational parameters of the hoisting installation are summarised in Table 1.

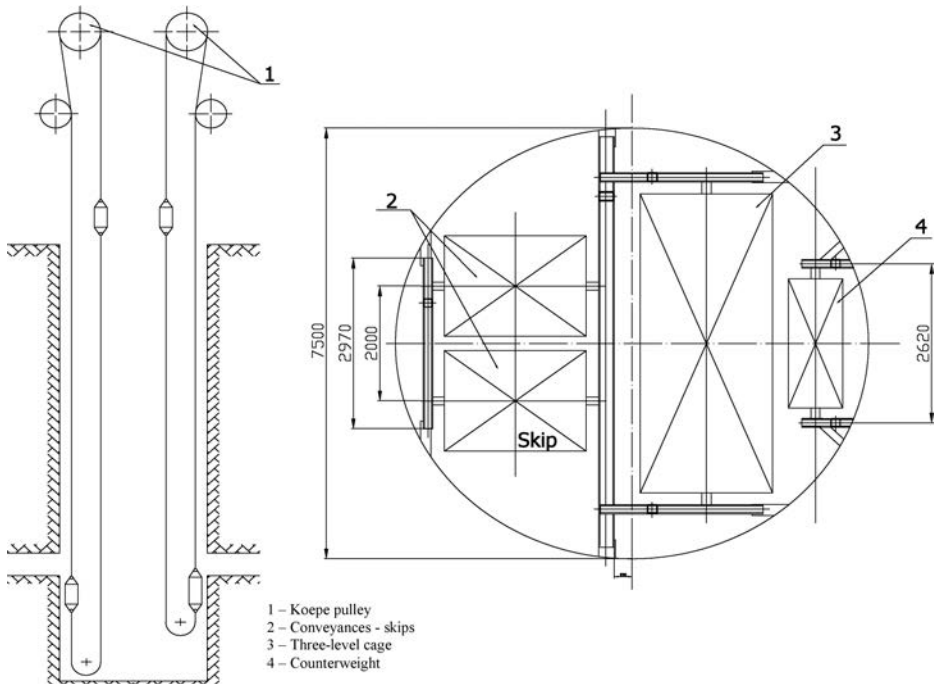


FIG. 1. Schematic diagram of the hoisting installation.

**Table 1.** Operational parameters of the hoisting installation used in the experiment.

Type	4L-4000/2900
Applied power /dc motor	2900 [kW]
Nominal rpm	77 rpm
Maximal skip velocity	$V = 16$ [m/s]
Conveyance and suspension	$m_{ku} = 16500$ [kg]
Payload	$m_u = 17000$ [kg]

The schematic diagram of the Koepe pulley is shown in Fig 2.

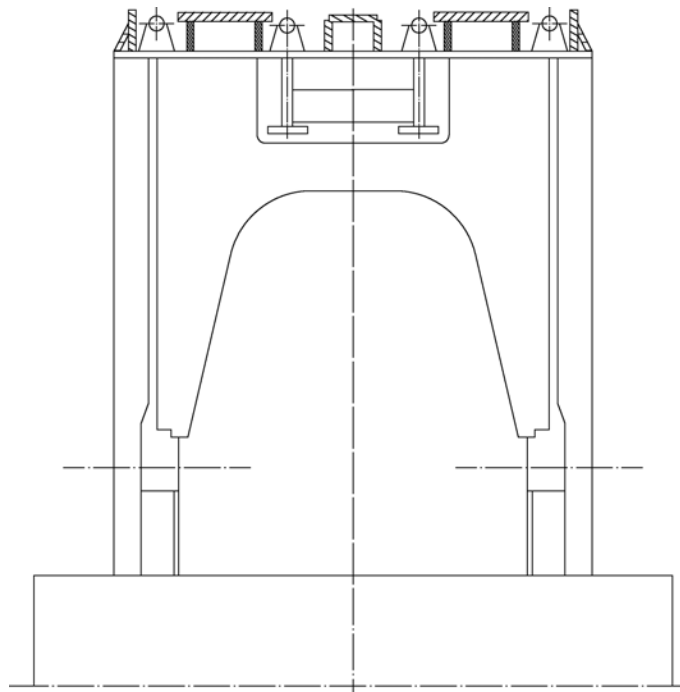


FIG. 2. Schematic diagram of the Koepe pulley.

The Koepe pulley has the major load-bearing elements (Fig. 3):

- a) short radial fins,
- b) side disc,
- c) hub,
- d) shaft,
- e) circumferential rings,
- f) mantle.

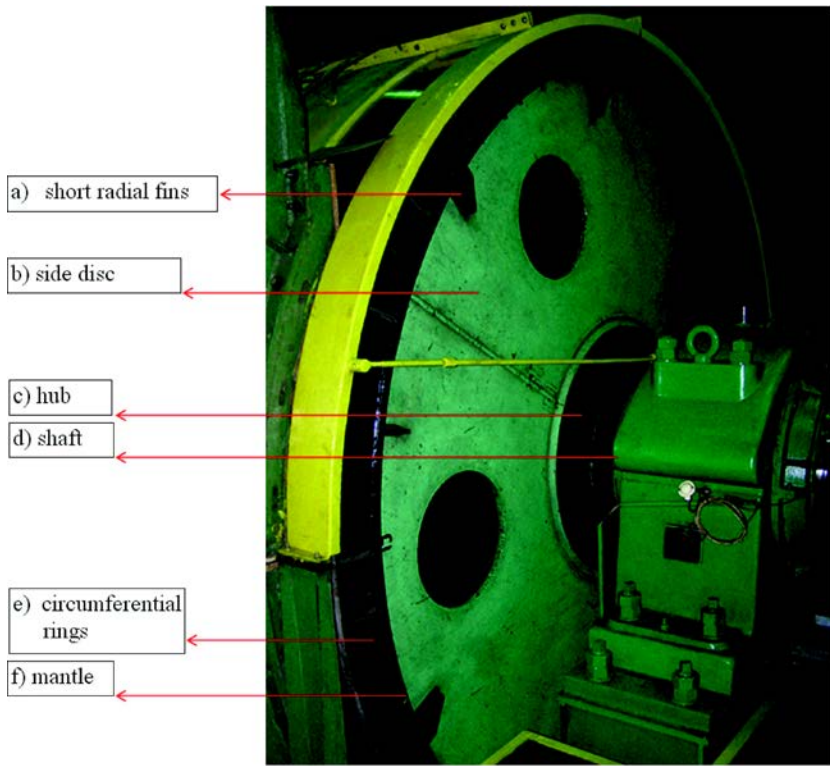


FIG. 3. Drum construction.

The Koepe pulley is a welded structure, made of steel grade St3S. The load is imposed by forces acting in hoisting ropes at the points they slid on and off the pulley during the normal duty cycle, derived from the dynamic analysis [3] verified by force measurements taken on a real object. Models are developed using the program "FEMAP" and the stress analysis uses the package "NE/Nastran for Windows". The numerical model uses 2D and 3D elements.

### *2.1. Calculation model*

To find the strain values and the state of stress in particular elements of the Koepe pulley, a numerical model is developed to capture the geometry of the tested structure (Fig. 4). The numerical model uses 2D and 3D (solid) elements.

The endurance analysis uses the package "NE/Nastran for Windows". Models are developed using the program "FEMAP". The model of the external part of the Koepe pulley (side discs, mantle, brake linings) is shown in Fig. 5, also revealing the shapes and layout of radial and circumferential fins. Figure 6 shows the positions of inspection opening reinforcements, the hub and the shaft.

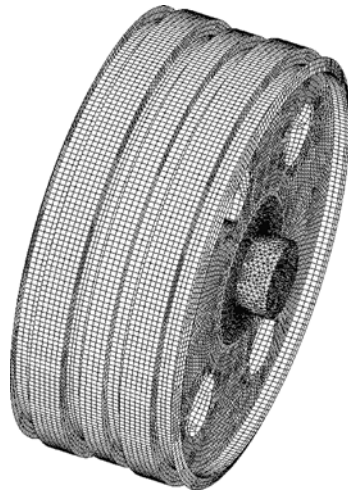


FIG. 4. Numerical model of the Koepe pulley.

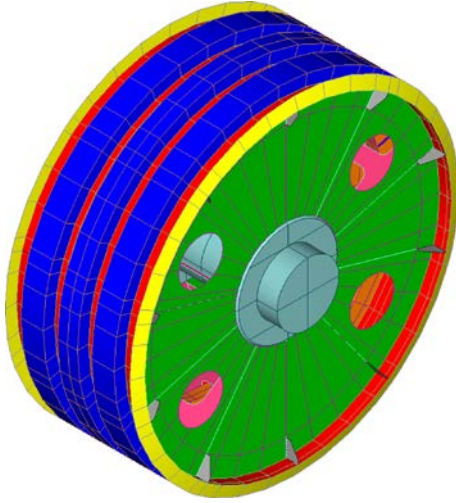


FIG. 5. Model of the drum 4L-4000/2900.

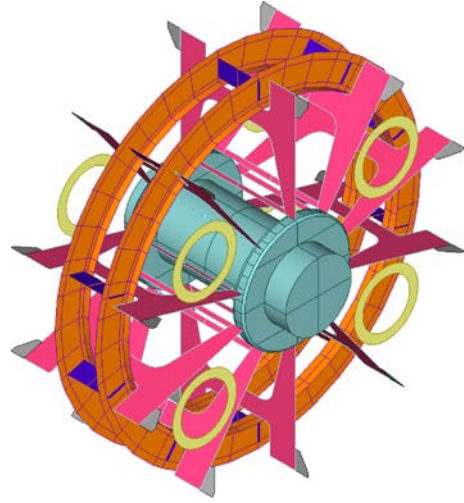
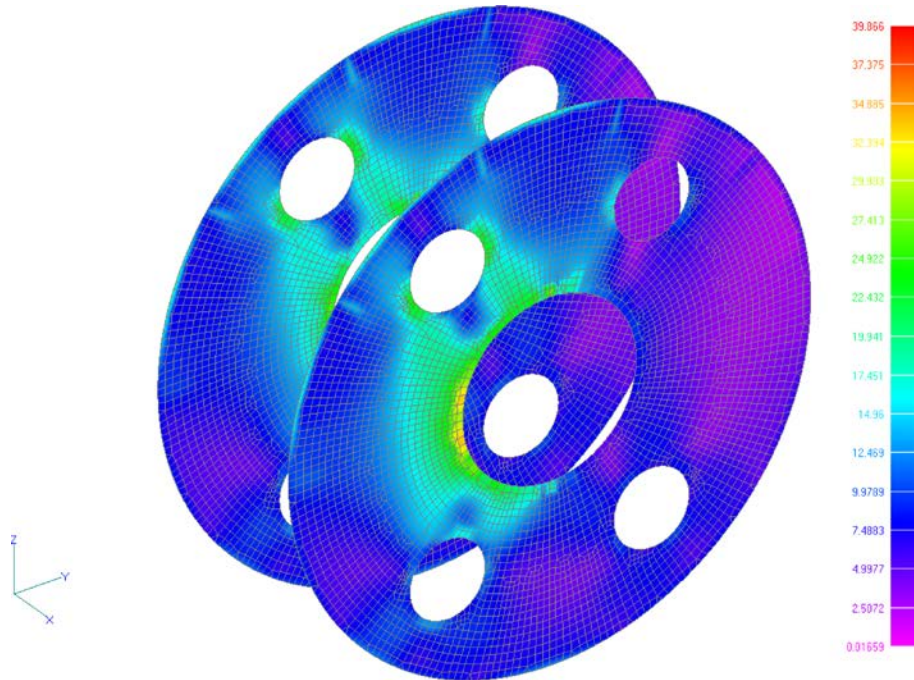
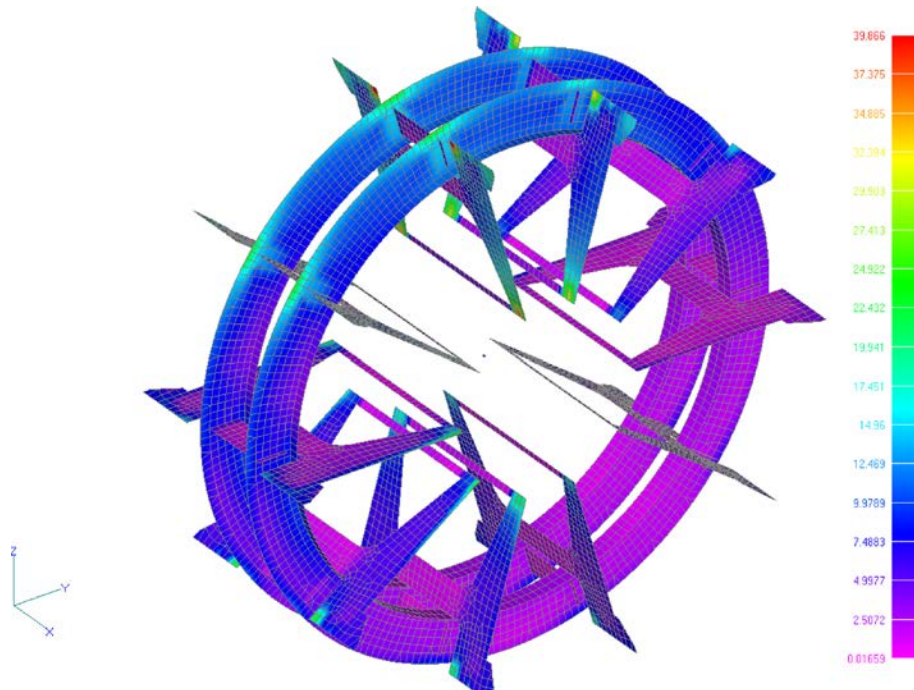


FIG. 6. Inside section of the Koepe pulley.

## 2.2. Results of strength analysis

Results of numerical analysis performed of the Koepe pulley components are shown in graphic form in Figs. 7–13. Figure 7 shows the distribution of reduced stress  $\sigma_z$  in side discs, based on the HMH hypothesis.

The largest reduced stresses in side discs, approaching 30 MPa are registered at points where they are connected to the rigid hub. Increased stress levels are also observed in the vicinity of inspection openings. Figure 8 shows the

FIG. 7. Reduced stress distribution  $\sigma_z$  on side discs.FIG. 8. Reduced stress distribution  $\sigma_z$  (Huber-von Mises) on radial and circumferential fins.

reduced stress distribution  $\sigma_z$  on radial and circumferential fins. The largest stress levels, approaching 40 MPa, are registered at points where they are welded to the mantle in the Koepe pulley. Further, the concentration of reduced stress (approaching 38 MPa, is registered at points where fins are connected to the hub. T-shaped circumferential fins exhibit a more uniform stress distribution over their entire area. Slight increase of stress is registered near the radial fins.

Rectangular supports fitted between the circumferential fins along the radius, just like radial fins, experience an increased stress at the point where they are welded to the circumferential fin. Figure 9 shows the reduced stress distribution on the surface of the mantle.

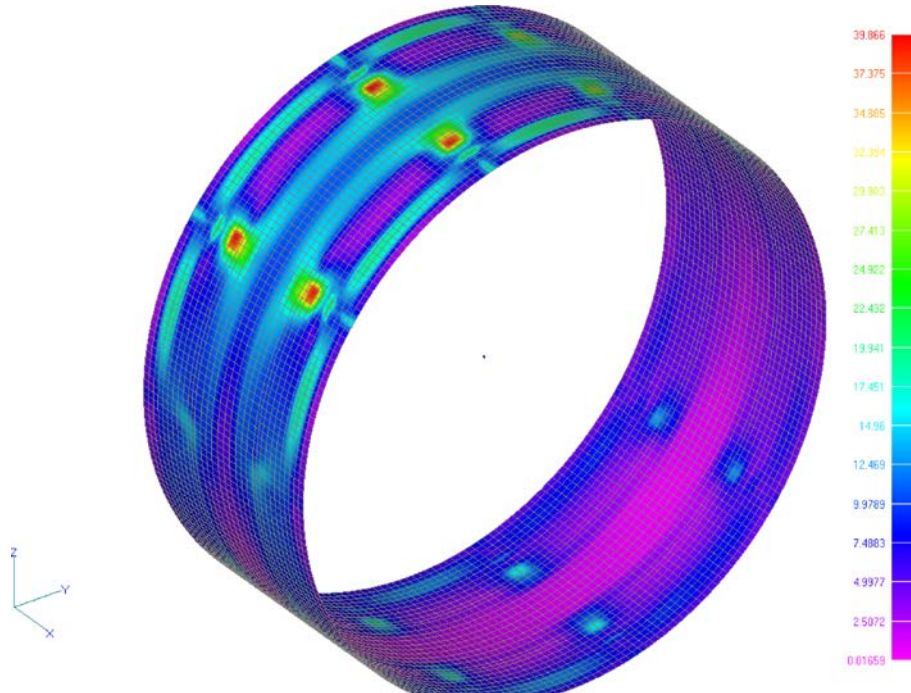


FIG. 9. Reduced stress distribution  $\sigma_z$  (Huber-von Mises) on the mantle's surface.

The largest stresses, approaching 40 MPa, occur at points where the mantle is connected to the radial fins. Figure 10 shows the reduced stress distribution at the point where the maximal material effort is registered on the mantle's surface during the full revolution of the Koepe pulley.

Cyclic stress increases are observed at the radial fin-mantle interface, which may cause the 'fatigue tester' effect, leading to endurance fatigue cracking.

Figure 11 shows the displacement of the pulley's mantle, the displacement pattern being re-scaled with respect to dimensions of the real construction for the sake of better visualisation. The maximal displacements, amounting to

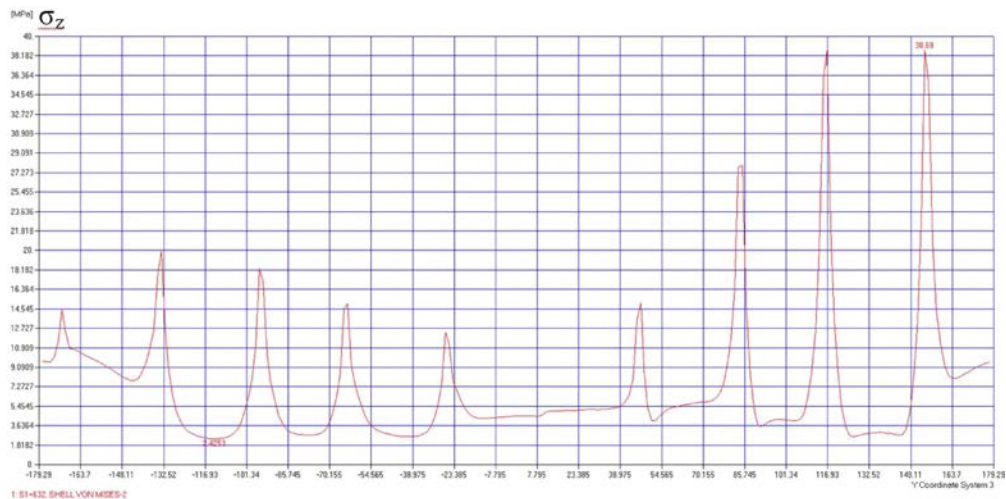


FIG. 10. Reduced stress distribution  $\sigma_z$  at the point where the maximal material effort is registered on the mantle's surface during the full revolution of the Koepe pulley.

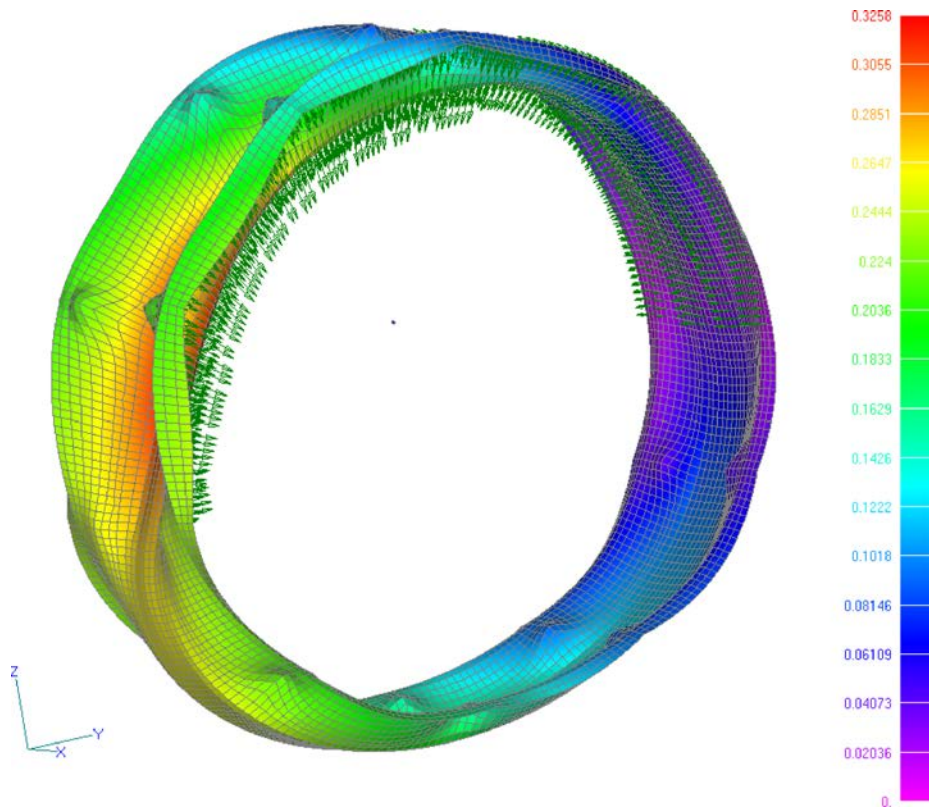


FIG. 11. Visualisation of the mantle's displacement.

0.3055 mm, are generated at points where hoisting ropes slid onto the pulley and the mantle is compressed (and pushed inwards) over the whole angle of lap. At points where no contact is maintained between the ropes and the pulley, the drum's mantle is under tension (and so it is pushed outwards the drum).

Figure 12 shows the reduced stress distribution on the hub and the drum's shaft.

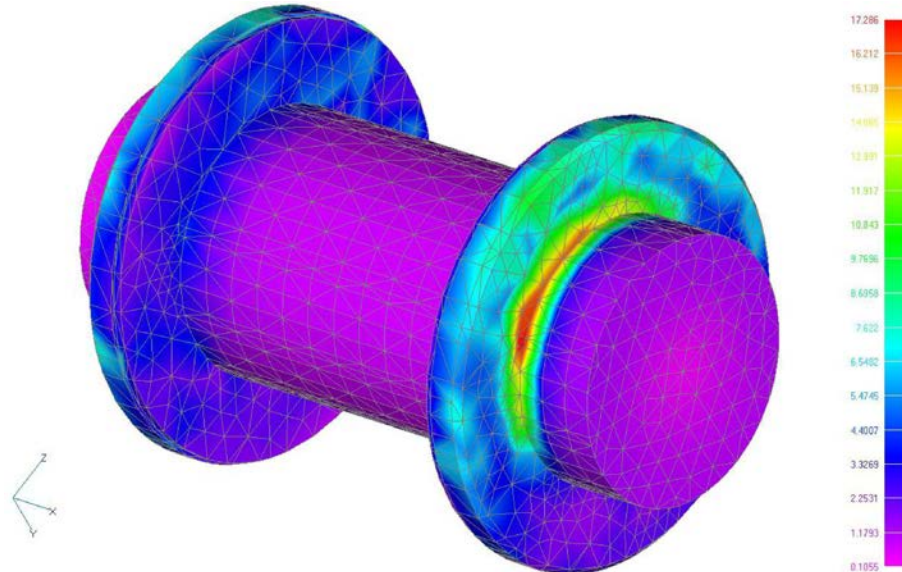


FIG. 12. Reduced stress distribution on the hub and the drum's shaft.

The maximal reduced stresses approach  $\sigma_z = 17.2$  [MPa] in the shaft-hub interface region.

### 3. STRAIN (STRESS) MEASUREMENTS ON A REAL OBJECT

The state of strain (stress) at the points where the maximal material effort is registered in the Koepe pulley and found by the numerical methods are verified by measurements taken on a real object.

#### 3.1. Measuring equipment

Measurements are taken with an amplifier HMB MGCplus utilising resistance or induction sensors. The bridge is supplied from gel batteries 12 V–12 Ah and the entire circuit is connected to a portable computer (laptop) supported by the professional programme “Catman” (HMB) to record the measurement data. The measurement equipment is shown in Fig. 13.



FIG. 13. Measuring equipment.

### 3.2. Measurement sensors (strain gauges)

Measurements are taken with two types of strain rosettes: TFxy-4/120 and TFr-8/120. Technical parameters of the strain rosette TFr-8/120 are summarised in Table 1. Strain rosettes TFxy-4/120 and TFr-8/120 are attached (glued) inside the Koepe pulley. The positions of control points (the spots where strain gauges are attached) are shown in Fig. 14.

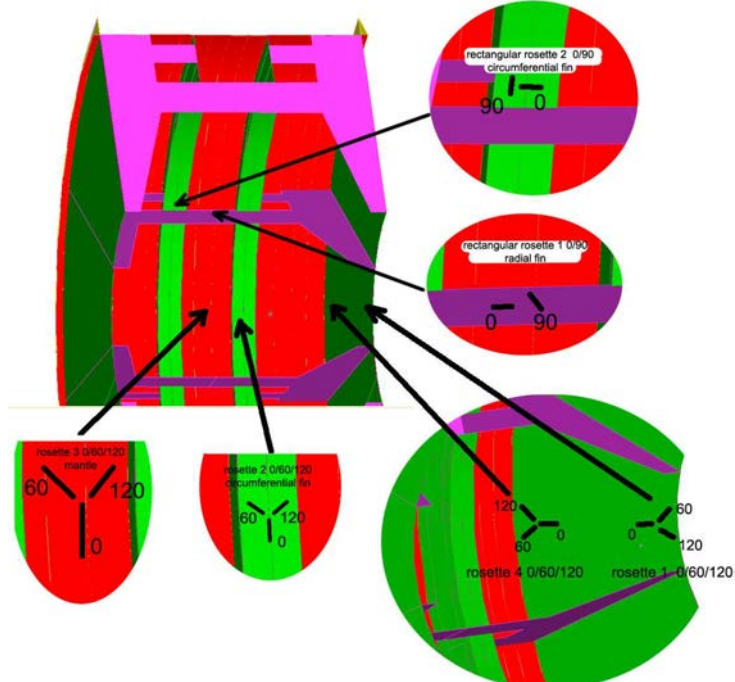


FIG. 14. Strain gauge attachment points inside the Koepe pulley.

The photo showing the location of strain sensors inside the construction of the Koepe pulley is shown in Fig. 15. The positions of strain gauges on radial and circumferential fins are shown in Fig. 16.

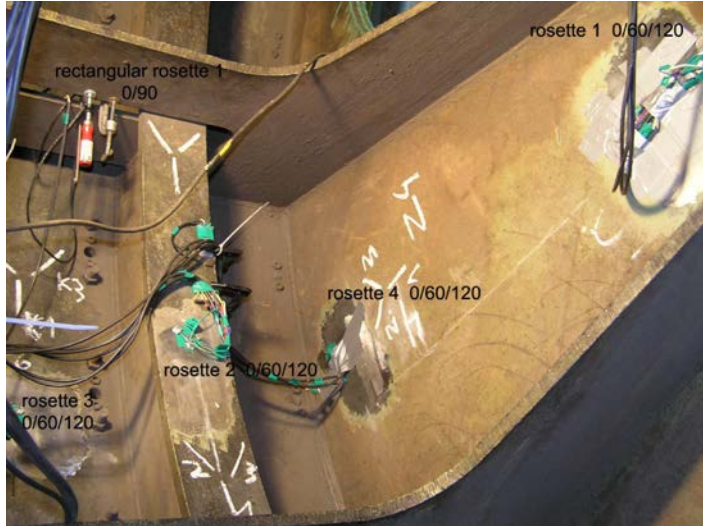


FIG. 15. Positions of strain gauges inside the Koepe pulley (photo).

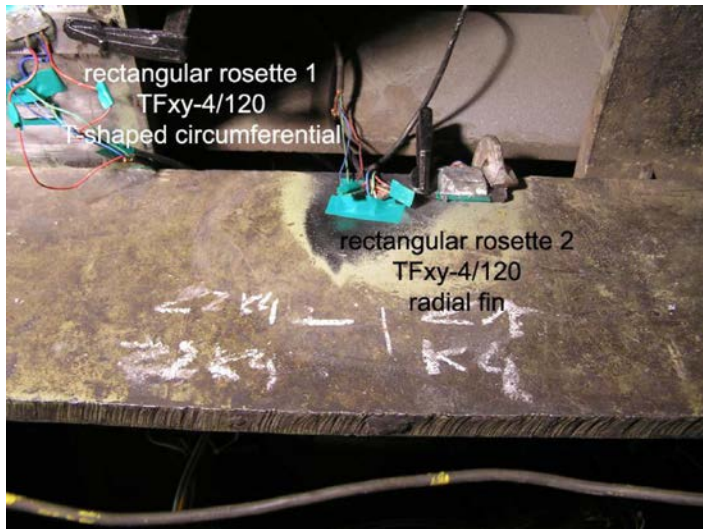


FIG. 16. Positions of strain gauges on radial and circumferential fins.

### 3.3. Measurement procedure

The measurement procedure uses 6 strain rosettes, including two rectangular rosettes TFxy-4/120. These rosettes have two active baselines perpendicular

to one another ( $0^\circ$ ,  $90^\circ$ ). Each strain gauge is temperature-compensated by a compensating gauge, identical as the one used for measurements (Fig. 15 – compensating boards fixed with hand screws). The strain sensors are attached (with a glue) to:

- circumferential fins – rectangular rosette No. 1 at the distance of 5 cm from the radial fin;
- centre point of the radial fin – rectangular rosette No. 2.

Strain rosettes TFxy-4/120 register 4 measurement signals altogether.

The remaining sensors include four rosettes TFr-8/120 with baselines arranged at the angles  $0^\circ$ ,  $60^\circ$ ,  $120^\circ$ . Each strain gauge is temperature-compensated. The sensors are attached to:

- side disc – rosette No. 1 at the distance of 10 cm from the hub,
- circumferential fin – rosette No. 2 in between radial fins (the sensor is arranged such that the baseline  $\varepsilon_0$  runs along the fin),
- the mantle in between the circumferential fins – rosette No. 3,
- side disc – at the distance of 10 cm from the drum's mantle – rosette No. 4.

Strain rosettes TFr-8/120 register 12 measurement signals altogether.

There are 16 channels from all strain gauges. The strain gauges are arranged such as to best capture the performance of vital pulley components, taking into account the variable duty cycles experienced in normal working conditions. The typical duty cycle of a hoisting installation is registered at the steady velocity  $v = 16$  m/s and during the emergency braking at  $v = 10$  m/s at the bottom level and half way up the shaft.

The measuring equipment is attached to the shaft inside the drum, in a special casing, to minimise the interactions of the centrifugal force. Data are recorded accordingly between particular measurement cycles, followed by assessment of the working condition of the connections and the equipment. Measurement data cover the full duty cycle of the hoisting installation, including ride down and ride up.

The strains  $\varepsilon_A$ ,  $\varepsilon_B$ ,  $\varepsilon_C$  along the directions  $0^\circ/60^\circ/120^\circ$  being derived from the formula (3.1) [1], the directions of principal stresses  $\sigma_1$  are obtained accordingly:

$$(3.1) \quad \sigma_1 = \frac{E}{3(1-v)} \left( \frac{\varepsilon_A + \varepsilon_B + \varepsilon_C}{3} \right) + \frac{3}{\sqrt{3}(1+v)} \sqrt{\frac{(2\varepsilon_A - \varepsilon_B - \varepsilon_C)^2}{3} + (\varepsilon_B + \varepsilon_C)^2}.$$

Figure 17 shows selected strain patterns registered by the strain rosette No. 2 during the full duty cycle of the hoisting installation (ride up and down), the skip travelling with the fixed velocity  $v_0 = 16$  [m/s].

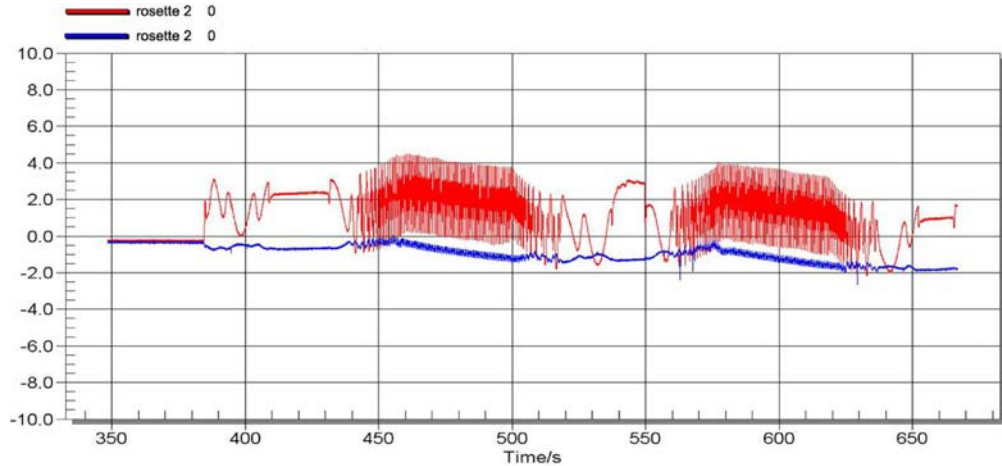


FIG. 17. Strains  $\varepsilon$  registered throughout the full duty cycle (ride down and up  $v_0 = 16$  [m/s]) by the rosette No. 2 along the directions  $\varepsilon_0$ ,  $\varepsilon_{60}$ .

Strains registered during the experiment by the strain rosette No. 1 along the directions  $\varepsilon_0$ ,  $\varepsilon_{60}$ ,  $\varepsilon_{120}$  are shown in Fig. 18.

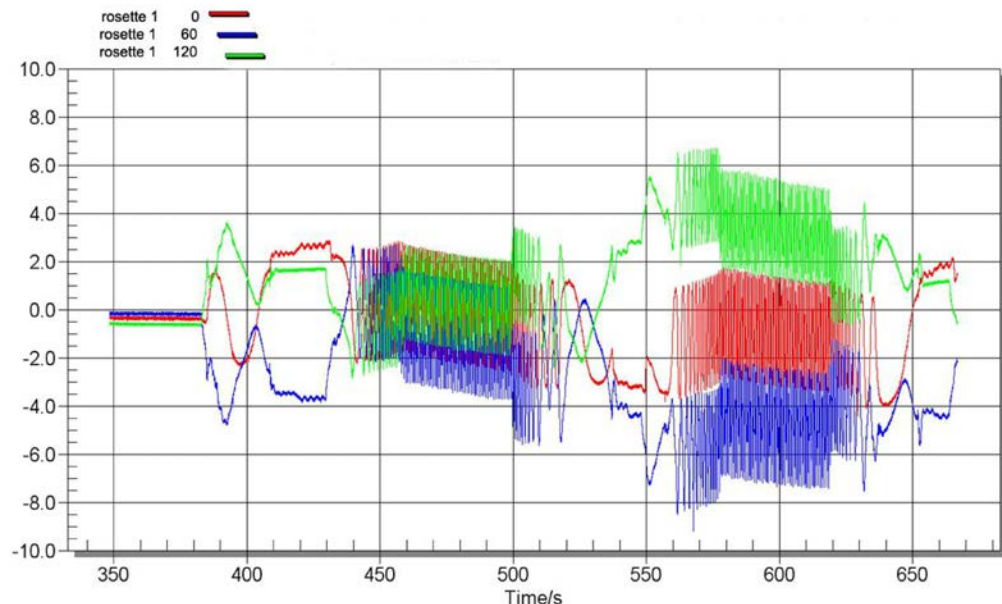


FIG. 18. Strains  $\varepsilon$  registered throughout the full duty cycle (ride down and up  $v = 16$  [m/s]) by the rosette No. 1 along the directions  $\varepsilon_0$ ,  $\varepsilon_{60}$ ,  $\varepsilon_{120}$ .

Figures 19 and 20 show the measured variations of the reduced stress throughout the typical duty cycle of the hoisting installation, registered by the following strain rosettes:

- strain rosette R1 (Fig. 19),
- strain rosette Pr2 (Fig. 20).

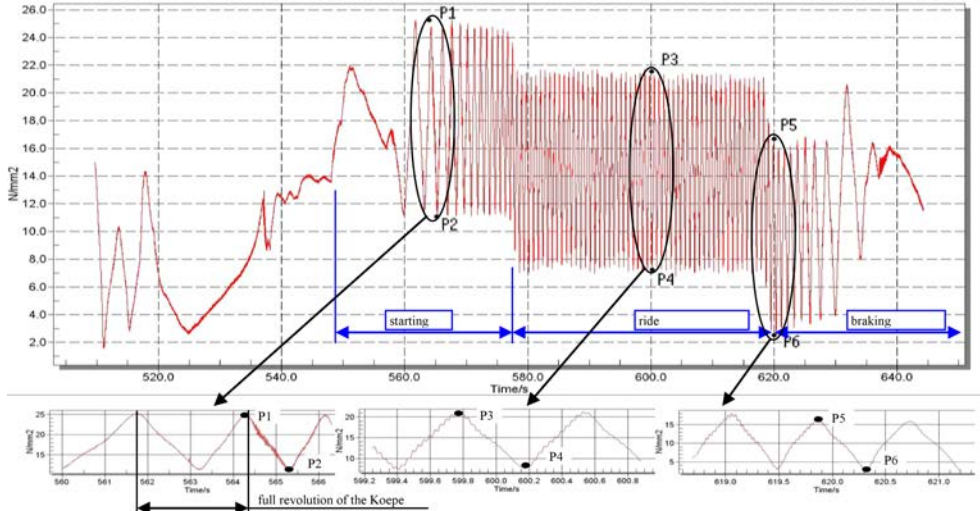


FIG. 19. Reduced stress  $\sigma_Z$  registered during the ride up of a fully loaded conveyance from the bottom station (strain rosette R1).

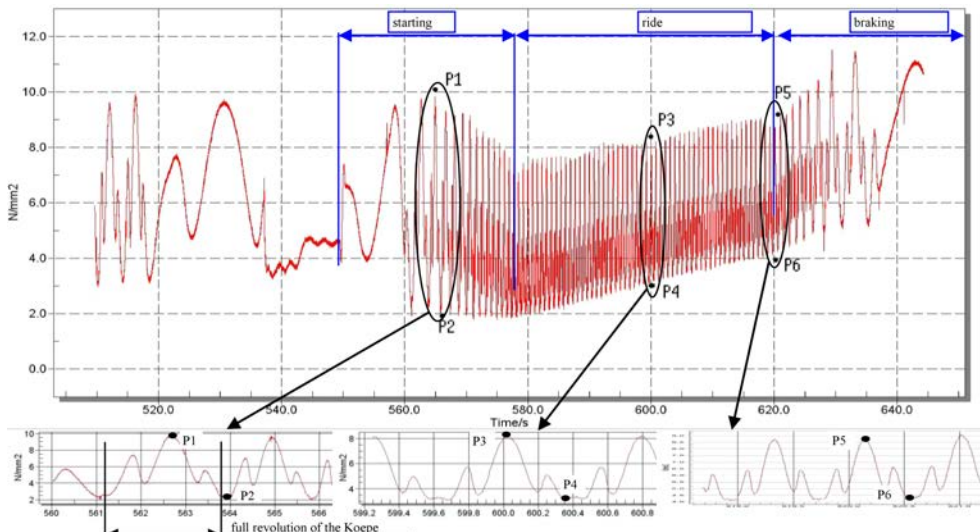


FIG. 20. Reduced stress  $\sigma_Z$  registered during the ride up of a fully loaded conveyance from the bottom station (strain rosette Pr2).

### 3.4. Numerical results and measurements taken on a real object

The adequacy of simplifying assumptions underlying the numerical analysis is verified through strain (stress) measurements taken on a real object. Reduced stresses  $\sigma_Z$  obtained from numerical analysis are compared with strain measurements taken on the real object, on the same points of the Koepe pulley construction (Fig. 21).

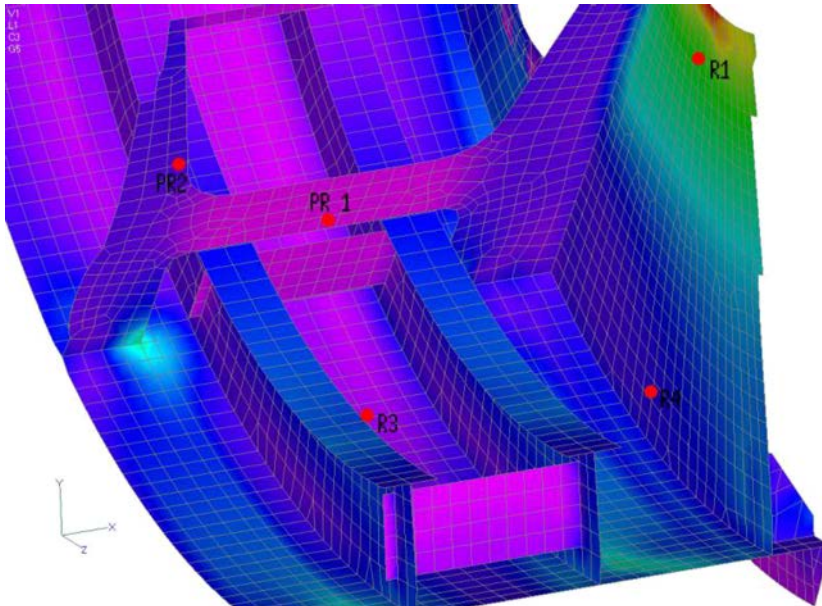


FIG. 21. Positions of readout points of reduced stress  $\sigma_Z$  in the numerical model (also the points where strain sensors are attached).

Amplitudes of reduced stresses obtained from the FEM analysis and from experiments on a real object are compared in Table 2. The data are registered during the ride-up of a fully loaded conveyance, moving from the bottom station with acceleration  $a_1$ , at the selected points of the pulley construction (Fig. 21).

**Table 2. Reduced stress amplitudes during the start-up of the conveyance.**

Strain gauge designation	$\Delta\sigma_Z$ [MPa]	
	FEM	Experimental
R1	16	18
R3	11	12.5
R4	10	9.5
Pr1	11.82	12.0
Pr2	10.5	8.9

#### 4. CONCLUSIONS

The numerical data agree well with measurement results, which on one hand confirms the adequacy of the assumptions underlying the strength analysis and on the other, proves the results to be reliable. Strength analyses have revealed that the stress values at nodes connecting the pulley components: circumferential fins to the mantle, the mantle with the side discs and the side discs with the hub determine the load-bearing capacity of the Koepe pulley.

Stress concentrations are mostly attributable to the presence of radial fins. If these were eliminated, those concentration points would disappear, however that cannot be done without a thorough stress analysis of Koepe pulley components to avoid the loss of stability.

#### REFERENCES

1. BADURA S., *Description of criterion of design of Koepe pulleys of winding gears*, AGH Kraków 2008.
2. WOLNY S., MATACHOWSKI F., *Analysis of loads and stresses in structural elements of hoisting installations in mines*, Engineering Transactions, **58**, 3–4, 153–174, 2010.
3. WOLNY S., *Dynamic loading of the pulley block in a hoisting installation in normal operating conditions*, Archives of Mining Sciences, ISSN 0860-7001, **54**, 2, 261–284, 2009.
4. WOLNY S., PŁACHNO M., *Experimental verification of bearing rope loading in typical operating conditions of the hoisting installation*, Archives of Mining Sciences, ISSN 0860-7001, **54**, 3, 531–542, 2009.

*Received September 29, 2011.*

---